

Single Underwater Image Restoration Using Adaptive Attenuation-Curve Prior

Yi Wang, Hui Liu, and Lap-Pui Chau, *Fellow, IEEE*

Abstract—Underwater imaging is an important topic in maritime research. Due to the existence of dust-like particles in water medium, underwater images are vulnerable to the effect of low contrast and color cast. In this paper, we propose a novel underwater image restoration method based on a non-local prior, namely, adaptive attenuation-curve prior. This prior relies on the statistical distribution of pixel values. That is, all pixel values of a clear image can be partitioned into several hundred distinct clusters in RGB space, and the pixel values in each cluster will be distributed on a curve with a power function form after attenuated by water in varying degrees. Specifically, we can estimate the transmission for each pixel according to its distribution on the curves. Then, we estimate the attenuation factor to compensate for the transmission. To prevent over saturation and reduce the noise of the recovered images, we propose the saturation constraints to adjust the transmission of the three color channels. Qualitative and quantitative results demonstrate that our proposed method can achieve better performance, compared with the state-of-the-art approaches. Moreover, our proposed method can be further extended to restore other kinds of degraded images, such as hazy images.

Index Terms—Underwater image, image restoration, light attenuation, attenuation-curve prior, transmission estimation, waterlight.

I. INTRODUCTION

UNDERWATER vision is one of the most fundamental parts in marine scientific research and ocean engineering, such as underwater imaging technology that helps subsea exploration to study marine biology and inspect geological environment. In addition, autonomous underwater vehicle (AUV) relies on vision methods to control itself in complicated condition. However, light attenuation poses a threat to high-quality underwater images/videos, which leads to haze-like surroundings for the underwater imaging system, and hinders most computer vision applications in the maritime environment [1].

The light attenuation is caused by scattering and absorption [2]. Because of the existence of dust-like particles floating around in the water, underwater images always suffer from

Manuscript received June 9, 2017; revised August 24, 2017 and September 5, 2017; accepted September 8, 2017. Date of publication September 26, 2017; date of current version February 15, 2018. This paper was recommended by Associate Editor H. Johansson. (Corresponding author: Lap-Pui Chau.)

Y. Wang and L.-P. Chau are with the School of Electrical and Electronics Engineering, Nanyang Technological University, Singapore 639798 (e-mail: wang_yi@ntu.edu.sg; elpcchau@ntu.edu.sg).

H. Liu is with the Maritime Institute, Nanyang Technological University, Singapore 639798 (e-mail: liuhui.csu@gmail.com).

Color versions of one or more of the figures in this paper are available online at <http://ieeexplore.ieee.org>.

Digital Object Identifier 10.1109/TCSI.2017.2751671

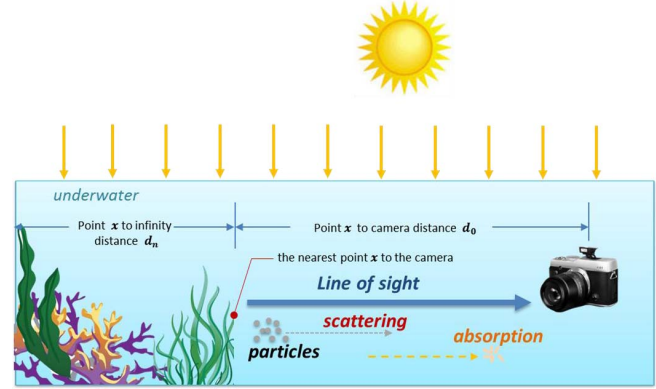


Fig. 1. Underwater scene of light propagation, airlight enters from air to the water, part of the light attenuates along the line of sight. The point x represents the nearest scene point to the camera.

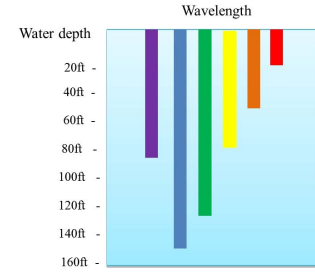


Fig. 2. Penetration of light with different wavelengths in the ocean.

the scattering effect. As shown in Fig. 1, light reflected from object surface travels to the camera, and scattering is formed when light interacts with particles suspended in the imaging medium. It can be subdivided into backscattering and forward scattering [1]. Backscattering occurs when the light from ambient illumination sources is scattered into the line of sight (LOS) and eventually reaches the image plane. This causes the haze-like waterlight for underwater images and greatly lowers the scene contrast. Forward scattering appears when part of reflected light spreads with small angles relative to LOS, which leads to image blur. Besides, as can be seen in Fig. 2, the light absorption rate in water varies with their wavelengths, so different colors of light will disappear gradually with the increase of the water depth. The water mostly absorbs the red light due to its longest wavelength. Conversely, the blue color has the smallest wavelength; it can penetrate the longest distance in water, so underwater images show a bluish or greenish tone. Therefore, low contrast and color distortion are two major problems we have to tackle.

To solve these problems, some previous works using the patch-based local priors have been proposed, e.g. adaptations of the dark channel prior (DCP) [3] or maximum intensity prior (MIP) [4]. However, they cannot achieve satisfactory results in both contrast enhancement and color restoration. Our previous work [5] proposed a non-local attenuation-curve prior and used it to enhance contrast and correct color for underwater images. In this paper, we have improved our previous work. The specific improvements are summarized as follows:

- 1) Compared with fixed attenuation-curve, we propose an adaptive attenuation-curve prior, which can model the attenuation process of light for different underwater scenes.
- 2) To get more accurate transmission, we divide it into two parts: the attenuation factor and the relative transmission, and estimate them respectively.
- 3) We set the saturation constraints to adjust the transmission to prevent over saturation and reduce the noise.
- 4) We give extensive experiments in the underwater and atmospheric environment to show the adaptability of the proposed method.

The flowchart of the proposed method is illustrated in Fig. 3. It consists of two main components: waterlight estimation and transmission estimation. First, we estimate the waterlight using the smoothness property and the wavelength-dependent attenuation of light and obtain attenuation ratios between color channels, which are key parameters for adaptively modeling the attenuation-curves in underwater environments. For transmission estimation, we estimate the initial relative transmission of red channel and refine it. Then, we calculate attenuation factor and adjust the transmission for the three color channels by the saturation constraints. Finally, the image can be restored by the waterlight and transmission.

The rest of the paper is organized as follows. In Section II, we review the previous works related to the underwater image restoration. In Section III, the underwater degeneration model and the adaptive attenuation-curve are presented deliberately. Our proposed underwater restoration method is described in detail in Section IV. The experimental results and analysis are reported in Section V. Finally, in Section VI, we give a conclusion of this paper.

II. RELATED WORK

Currently, many approaches have been proposed to address the above mentioned problems for enhancing the underwater vision. The approaches can be classified into two categories. One is the image restoration method that attempts to recover the degraded images using the image formation model (IFM) [1]. Recently the most widely used IFM is based on the DCP [3] that was employed to dehaze images taken in the atmosphere. Similarly, the underwater image formation can also be considered as a distance-based degradation problem. Therefore, the DCP can also be improved to adapt to the underwater situation and many underwater DCP-based methods have been proposed. Chiang and Chen [2] enhance underwater images by applying the DCP for dehazing and using wavelength compensation for color restoration.

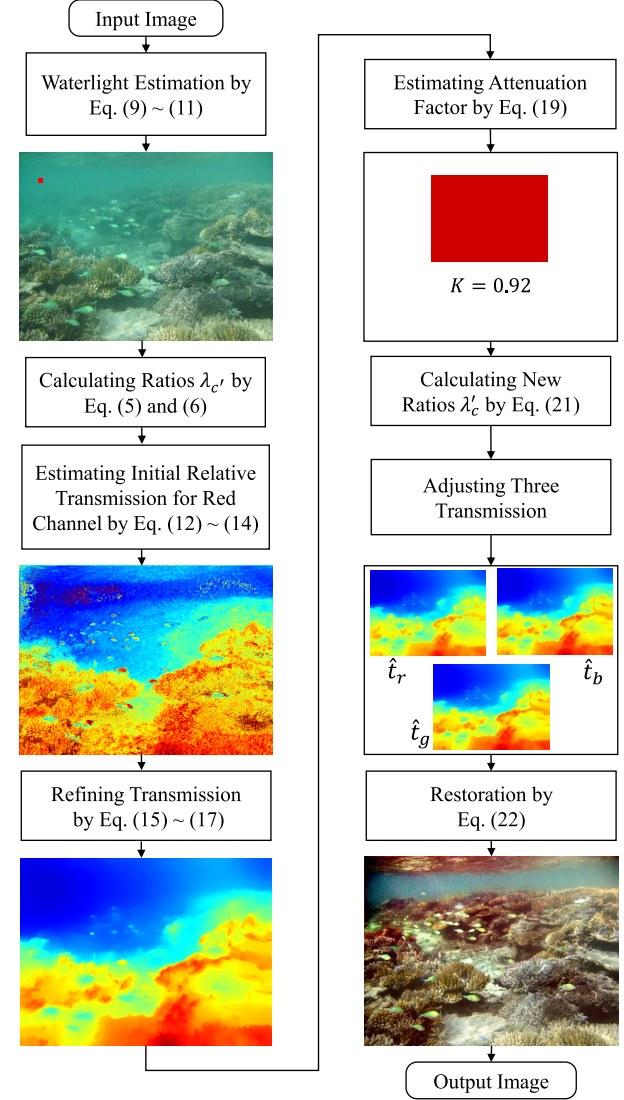


Fig. 3. The flowchart of the proposed method.

Analogously, Wen *et al.* [6] derived a new underwater optical model based on DCP to enhance the underwater images. Galdran *et al.* [7] proposed a red channel prior to restore the underwater image. Drews *et al.* [8] presented a underwater dark channel prior (UDCP) to estimate the transmission map for underwater images. In addition, Carlevaris-Bianco *et al.* [4] proposed the MIP, which is based on the fact that there is a large difference in attenuation among three image color channels in the water, and utilized it to estimate the underwater transmission map. However, most of the time, neither the above DCP-based nor MIP-based methods can achieve satisfactory restoration results due to the varying lighting conditions in underwater imaging. To improve those methods, Peng and Cosman [9] proposed a depth estimation method for underwater images based on image blurriness and light absorption. In summary, those techniques are theoretically rigorous but not feasible in practice because they depend much on estimating some key parameters in the physical model, such as the light scattering and absorption coefficients which may change considerably in different types of water.

Another kind is the non-IFM image enhancement technique such as the histogram-equalization-based methods, white balance, retinex-based and fusion-based approaches. Getreuer [10] proposed a novel method called automatic color enhancement (ACE) that is based on the mechanism of the human visual system. ACE tries to model some adaptation mechanisms such as the lightness constancy and color constancy of the human vision system. Ancuti *et al.* [11] presented an effective underwater image enhancement method by fusion and blends various filters to rebuild a clear image. A method in [12] is based on the retinex theory [13] for enhancing underwater images. Methods of this kind do not need any IFM (like scattering and absorption coefficients) but only use the qualitative subjective criteria to produce enhanced images. These approaches are usually easier to implement than the physical model based methods. However, this kind of enhancement techniques may produce visually unnatural results (like over saturation or over enhancement) and is not sufficient for underwater images with different physical properties.

III. UNDERWATER IMAGE MODELING AND ADAPTIVE ATTENUATION-CURVE PRIOR

In this section, we first introduce a degradation model for underwater images with analysis of its characteristics. Then, we propose a novel adaptive attenuation-curve prior to describe the degeneration process for underwater images.

A. Modeling of Underwater Images

Similar to the degradation model of images captured in atmospheric environments [3], [14], the degeneration process for underwater images can be generally formulated as:

$$I_c(x) = t_c(x) \cdot J_c(x) + (1 - t_c(x)) \cdot B_c, \quad c \in \{r, g, b\}, \quad (1)$$

where x represents pixel coordinates, c is the color channel index, I denotes the observed image, J denotes the scene radiance, i.e., the clear image, B denotes the waterlight determined by ambient illumination, and t is the medium transmission. The first term on the right-hand side of Eq. (1) is called *direct attenuation* that interprets the degradation of the scene radiance in the medium [3]. The second term is called *waterlight shift* which defines the shift from scene radiance to waterlight.

The transmission $t_c(x)$ relies on the scene depth $d(x)$ and wavelength-dependent attenuation coefficient β_c :

$$t_c(x) = e^{-\beta_c d(x)} = e^{-(a_c + s_c)d(x)}, \quad c \in \{r, g, b\}, \quad (2)$$

where $\beta = a + s$ with a and s being the absorption and scattering coefficients, respectively. To get more accurate transmission, we represent the scene depth d as the summation of two distances, i.e., d_0 , the distance between the camera and the closest scene point, and d_n , the distance between the closest scene point and the farthest scene point as shown in Fig. 1. Thus, Eq. (2) can be rewritten as:

$$t_c(x) = e^{-\beta_c d_0} \cdot e^{-\beta_c d_n(x)} = K_c \cdot t_c^n(x), \quad c \in \{r, g, b\}, \quad (3)$$

where $K_c = e^{-\beta_c d_0}$ is a constant attenuation factor, and $t_c^n = e^{-\beta_c d_n(x)}$ is named relative transmission.

Moreover, the transmission of green and blue channels exhibits a power function relationship with the transmission of the red channel [7]:

$$t_{c'}(x) = e^{-\beta_{c'} d(x)} = \left(e^{-\beta_r d(x)} \right)^{\beta_{c'}/\beta_r} = t_r(x)^{\lambda_{c'}}, \quad (4)$$

where $c' \in \{g, b\}$, and $\lambda_g = \beta_g/\beta_r$ and $\lambda_b = \beta_b/\beta_r$ are attenuation ratios between color channels. They are equal to one in the atmospheric environment, but they are not equal to one in the underwater environment most of the time.

The absorption coefficient a varies irregularly with the light wavelength, while the scattering coefficient s changes little for different types of water, e.g., case 1 and case 2 waters [15]. Particularly, for red, green, and blue lights, the quantitative relationship between their scattering coefficients towards some certain types of water has been derived via the least-square regression [15]:

$$\frac{s_{c'}}{s_r} = \frac{-0.00113\Lambda_{c'} + 1.6251}{-0.00113\Lambda_r + 1.6251}, \quad c' \in \{g, b\}, \quad (5)$$

where we choose three standard wavelengths $\Lambda_r = 620\text{ nm}$, $\Lambda_g = 540\text{ nm}$, $\Lambda_b = 450\text{ nm}$ for red, green and blue lights, respectively. Furthermore, based on inherent optical properties, we can calculate the attenuation ratios $\lambda_{c'}$ between color channels [16]:

$$\lambda_{c'} = \frac{\beta_{c'}}{\beta_r} = \frac{s_{c'}}{s_r} \cdot \frac{B_r}{B_{c'}}, \quad c' \in \{g, b\}. \quad (6)$$

It can be observed that the reliability of λ_g and λ_b depends on the accuracy of the estimated waterlight B . In the paper, even if we get inaccurate ratios by Eq. (6), we still can use them to build attenuation-curve clusters in RGB space and estimate the initial transmission. This is because the transmission estimation for curves is robust even though the ratios fluctuate. However, the ratios can make a big difference in calculating the final transmission for the three color channels. The inaccurate estimation of the ratios might make the images looks dim or over saturated, and even decreases the contrast of some color channels of restored images. We will describe the saturation constraints to calculate the new ratios for recovering images. To sum up, in this kind of ill-posed problem, we only know the observed image, and our purpose is to restore the scene radiance by estimating the waterlight and transmission.

B. Adaptive Attenuation-Curve Prior

The non-local Haze-Line prior in [17] that describes the change between the clear image J and the observed image I . However, in the underwater environment, the change is much more complicated to deal with. The reason is that dust-like particles in the medium lead to wavelength-dependent attenuation coefficients. According to Eq. (2), the transmission $t_c(x)$ depends on both the distance and wavelength. We propose a more general prior, namely adaptive attenuation-curve prior, for various imaging environments, like haze, fog and water.

We define that pixels with similar colors belong to the same cluster towards a clear image. For the clear outdoor

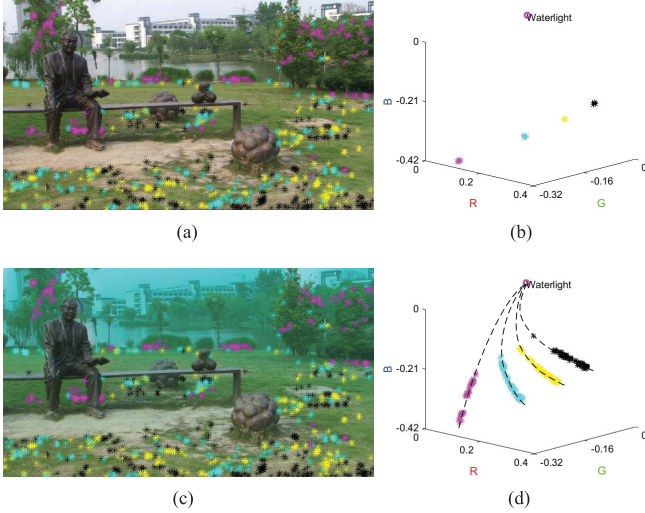


Fig. 4. Attenuation-Curve Prior. (a) Four clusters' pixels in the clear image. (b) Corresponding clusters with different locations in RGB space. (c) The synthetic image with the same clusters. (d) Corresponding attenuation-curves in RGB space.

natural image, the work in [17] has verified that several hundred color clusters can represent all colors of the image with the acceptable result. They validated it on the BSDS300 dataset. Specifically, they used K-means to find 500 clusters for each image and renewed every pixel value with its corresponding cluster center. The generated images had satisfactory PSNR with 36.6dB to 52.6dB. The observation is also valid for underwater images.

In the underwater environment, there are two factors affecting the change between clear image and the observed image: the varying scene depth $d(x)$ from the camera to objects, which leads to the difference of transmission $t(x)$ for every pixel, and the wavelength-dependent attenuation coefficient β_c , which results in the difference of three elements in transmission vector, generating $t_c(x)$. Because of these two factors, based on Eq. (1), the scene radiance $J_c(x)$ from the same cluster (with similar original colors) is attenuated in varying degrees, thereby generating different captured colors $I_c(x)$ in the observed image. If we depict every pixel value of the cluster in RGB space, due to the varying depths from the camera, the pixel values will form a line, which starts from the original color J (if $t = 1$) and ends at the waterlight color B (if $t = 0$). The wavelength-dependent attenuation coefficient will bend the line into a power function curve according to Eq. (4) as shown in Fig. 4. Therefore, we name it as an attenuation-curve.

The prior can be explained by substituting Eq. (4) into Eq. (1) as follow:

$$(I_{c'} - B_{c'}) = (I_r - B_r)^{\lambda_{c'}} \cdot \frac{J_{c'} - B_{c'}}{(J_r - B_r)^{\lambda_{c'}}}, \quad c' \in \{g, b\}. \quad (7)$$

If we define the RGB coordinate space with the waterlight as the origin, the intensity of the green or blue channel ($I_{c'} - B_{c'}$) of the observed pixels has a power function relationship with that of the red channel ($I_r - B_r$). Because the values of B and $\lambda_{c'}$ are constants for a certain underwater scene, the curve

uniquely relies on the scene radiance J . Different J corresponds to the different curve. So, the formation of attenuation-curves can model the degeneration process for underwater images and adapt to different underwater scenes according to Eq. (6).

The prior is illustrated in Fig. 4. Fig. 4(a) shows that pixels of a clear image are clustered, and four of them are marked by four colors. In RGB space, four clusters center on four different locations as shown in Fig. 4(b), in which color markers correspond to Fig. 4(a). We synthesize an observed image using Eq. (1) and Eq. (4) by setting $B = [0.16, 0.66, 0.58]$, $\lambda_g = 0.34$ and $\lambda_b = 0.27$, getting the ground truth t_r [18]. Fig. 4(c) shows the synthetic image with the same clusters as Fig. 4(a), but for each cluster, their observed colors are different from original ones because of the varying scene depth and different attenuation coefficients of the three color channels. The changes can be seen in RGB space in Fig. 4(d). Each curve consists of different observed colors, which should belong to the same cluster in the clear image. Combining Eq. (3), it can also guarantee the power function relationship:

$$(I_{c'} - B_{c'}) = (I_r - B_r)^{\lambda_{c'}} \cdot \frac{K_{c'}(J_c - B_{c'})}{[K_r(J_r - B_r)]^{\lambda_{c'}}}, \quad c' \in \{g, b\}. \quad (8)$$

We will use the prior to cluster pixel values into curves and estimate per-pixel transmission for each curve in the following section.

IV. UNDERWATER IMAGE RESTORATION

In this section, we propose a novel and effective underwater image restoration method based on the adaptive attenuation-curve prior. It is composed of two main components: waterlight estimation and transmission estimation.

A. Waterlight Estimation

The waterlight B refers to the homogeneous background light, arising from backscattering. Generally, it can be estimated from the pixels belonging to background regions and with a low variance. To estimate B more accurately, we first empirically partition the degraded image into overlapping patches, and then choose the patches with the total variation (TV, which calculated by $TV(P) = \sum_x \|\nabla P(x)\|_1$, where P stands for image patch) less than a predefined threshold.

Within the smooth patches, we calculate the differences between the intensity of the red channel and the green or blue channels:

$$D_{c'}(x) = I_{c'}(x) - I_r(x), \quad c' \in \{g, b\}, \quad (9)$$

where $x \in S$, $S = \{\text{all pixels in the chosen patches}\}$. Because the red light attenuates more rapidly than the green and blue light in the water, those differences for the waterlight are consistently larger. Thus, if R-G channel and R-B channel of a pixel have considerable differences, it is very likely that the pixel is a candidate for the waterlight.

To find the pixel, we use the index function $\text{Ind}(\cdot)$ to sort the differences D_g and D_b in descending order (e.g., $\text{Ind}_{c'}(1)$

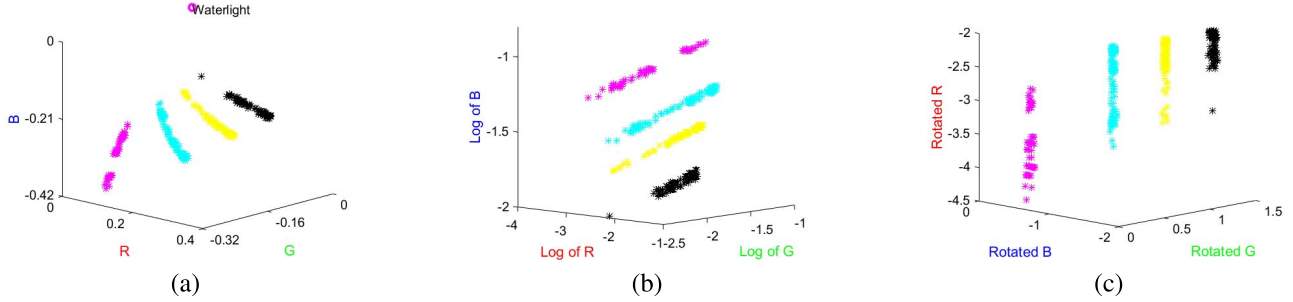


Fig. 5. Finding Attenuation-Curves. (a) The power function relationship between color channels. (b) The linear relationship. (c) Rotated coordinates for clustering.

are coordinates of the pixel with the maximum value in $D_{c'}$:

$$\text{Ind}_{c'}(n) = \text{sort}(D_{c'}(x)), \quad c' \in \{g, b\}, \quad (10)$$

where $\text{Ind}_{c'}(n)$ outputs indexes (coordinates) of the sort. The intersection $Z = \text{Ind}_g(n \leq N) \cap \text{Ind}_b(n \leq N)$ can obtain the indexes with the largest values in both D_g and D_b , where N is a parameter to control the number of the intersection's elements. Thus, the final estimated waterlight B is expressed as:

$$B_c = I_c \left(\arg \max_{x \in Z} I_c(x) \right), \quad c \in \{r, g, b\}. \quad (11)$$

We consider a pixel with the maximum value of the red channel as the waterlight. The small red rectangle in Fig. 3 indicates the selected waterlight.

B. Transmission Estimation

According to Eq. (3), the transmission estimation is composed of two parts: relative transmission t_c^n estimation and attenuation factor K_c estimation. The first part is to estimate the relative transmission for the distance between the farthest scene point and the nearest scene point, while the second part is to estimate the attenuation from the nearest scene point to the camera. We divide it into five steps: finding attenuation-curves, estimating an initial relative transmission t_c^n , refining the transmission, estimating attenuation factor K_c , adjusting the transmission of three color channels.

1) *Finding Attenuation-Curves:* According to the proposed prior, we need to classify the pixels of the image into the attenuation-curves in RGB space as shown in Fig. 5 (where four of them are depicted). However, it is challenging and inefficient to cluster pixels into curves by their RGB coordinates directly. To facilitate this task, we calculate logarithm for Eq. (8):

$$\ln |I_{c'} - B_{c'}| = \lambda_{c'} \ln |I_r - B_r| + \ln \frac{K_{c'} |J_{c'} - B_{c'}|}{(K_r |J_r - B_r|)^{\lambda_{c'}}}, \quad c' \in \{g, b\}. \quad (12)$$

Compared to the power function relationship, $\ln |I_{c'} - B_{c'}|$ and $\ln |I_r - B_r|$ follow the linear relationship in RGB space. The straight lines have the same slope $\lambda_{c'}$ but different intercepts. The scene radiance J determines the intercept. Instead of clustering the pixels into curves, we can classify

them into the lines. Four curves turn into the lines using logarithm as shown in Fig. 5(b).

To speed up the clustering process, we rotate the 3D coordinate system to make the R-axis parallel to the direction of the straight lines. In the new coordinate system, it is efficient to cluster the pixels by building a KD-Tree from the predefined tessellation in the rotated G-B plane and querying the tree from their rotated G and B coordinates. Fig. 5(c) shows the clusters in the rotated RGB system. Finding attenuation-curves only need pixels' rotated G and B coordinates.

2) *Estimating an Initial Relative Transmission t_c^n :* After finding the attenuation-curves, we estimate the initial relative transmission for the pixels in each curve. We reformulate the model (Eq. (1)) as:

$$|I_c(x) - B_c| = t_c^n(x) \cdot K_c |J_c(x) - B_c|, \quad x \in L, \quad c \in \{r, g, b\}, \quad (13)$$

where L is a curve, so $x \in L$ stands for the pixels belonging to the curve. For each curve, if $t_c^n(x) \rightarrow 1$, the intensity of the pixel $I_c(x)$ is nearer to the degraded scene radiance $K_c J_c(x)$, while if $t_c^n(x) \rightarrow 0$, the $I_c(x)$ is nearer to the waterlight B_c . So, the maximum value of $|I_c(x) - B_c|$ in a curve is the nearest to $K_c |J_c(x) - B_c|$. We consider it as the estimation of $K_c |J_c(x) - B_c|$ and obtain per-pixel transmission $\tilde{t}_c^n(x)$ for each curve by:

$$\tilde{t}_c^n(x) = |I_c(x) - B_c| / \max_{x \in L} |I_c(x) - B_c|, \quad c \in \{r, g, b\}. \quad (14)$$

Instead of estimating $|J_c - B_c|$ [5], we use the maximum value of $|I_c - B_c|$ to estimate $K_c |J_c - B_c|$, which is much closer to $K_c |J_c - B_c|$ ($K_c < 1$) than $|J_c - B_c|$ and more accurate than that in [5]. This is because the maximum value of $|I_c - B_c|$ represents the nearest scene point, in which scene radiance has been degraded by K_c .

According to Eq. (6), λ_g and λ_b are given, and we only need to estimate the transmission of one color channel because the transmission of the green and blue channel can be calculated by Eq. (4). In this paper, we calculate the transmission of the red channel $\tilde{t}_r^n(x)$.

3) *Refining the Relative Transmission:* Although the above method can obtain the initial transmission, the assumption we use to estimate the value of $K_c |J_c - B_c|$ may be wrong if the curve is very short and close to the waterlight, such as the distant background area of the initial transmission

in Fig. 3. Based on smoothness observation of the depth, the transmission map should be patch-wise smooth apart from the depth discontinuities [17]. The transmission is refined by applying the WLS filter [17], [19]:

$$\min_{\hat{t}_r^n(x)} \sum_x \frac{[\hat{t}_r^n(x) - \tilde{t}_r^n(x)]^2}{\sigma_r^2(x)} + \lambda \sum_x \sum_{y \in N_x} \frac{[\hat{t}_r^n(x) - \hat{t}_r^n(y)]^2}{\|I(x) - I(y)\|^2}, \quad (15)$$

where $\hat{t}_r^n(x)$ is the refined transmission, λ is a regularization parameter to adjust the data and the smoothness terms, N_x is the four nearest neighbors of x , and $\sigma_r(x)$ is a parameter to measure the reliability of the assumption for $\hat{t}_r^n(x)$.

Two factors determine $\sigma_r(x)$. For each curve, we consider the standard deviation $\text{std}_{x \in L}(I_r(x))$ for the red channel of pixels located on the curve L . We normalize the standard deviation of each curve by the maximum of standard deviations, and get: $\tilde{\text{std}}_{x \in L}(I_r(x))$. Higher deviation of the curve means that the assumption for $\hat{t}_r^n(x)$ is more reliable. Besides, we take into account the number of pixels in each curve $n(L)$. More pixels in the curve implies that the assumption for $\hat{t}_r^n(x)$ is more reliable. We define the count reliability for each curve as:

$$\text{count_reliability}(L) = \min(1, n(L)/50). \quad (16)$$

By combining those two factors, the reliability parameter $\sigma_r(x)$ for each curve L can be obtained as:

$$\frac{1}{\sigma_r(x)} \propto \tilde{\text{std}}_{x \in L}(I_r(x)) \cdot \text{count_reliability}(L). \quad (17)$$

As described in [17], a larger value of $1/\sigma_r(x)$ makes the assumption for $\hat{t}_r^n(x)$ more reliable since the first term of Eq. (15) will make a significant contribution to the initial relative transmission refining. That is, the refined transmission is close to the initial transmission ($\hat{t}_r^n(x) \rightarrow \tilde{t}_r^n(x)$), rather than being smoothed by the neighboring transmission (the second term of Eq. (15)).

4) *Estimating Attenuation Factor K_c* : Based on the observation of clear outdoor images, we assume there must be the brightest or darkest pixel α in one of three color channels ($J_c(x = \alpha) = 1$ or 0). Formally, there exists a pixel α satisfying the equation:

$$\max_{c \in \{r, g, b\}} \frac{|J_c(\alpha) - B_c|}{\max(B_c, 1 - B_c)} = 1. \quad (18)$$

Similarly to Eq. (14), $K_c |J_c(\alpha) - B_c|$ can be estimated by $\max |I_c(x) - B_c|$ for all pixels in the image. We simplify three attenuation factors with one factor ($K_c = K$). So, we substitute $K |J_c(\alpha) - B_c| = \max |I_c(x) - B_c|$ into Eq. (18) and get:

$$K = \max_{c \in \{r, g, b\}} \frac{\max |I_c(x) - B_c|}{\max(B_c, 1 - B_c)}. \quad (19)$$

After getting the relative transmission $\hat{t}_r^n(x)$ and the attenuation factor K , we can recover the transmission $\hat{t}_r(x)$ by Eq.(3).

5) *Adjusting the Transmission of Three Color Channels*: Via the transmission of the red channel, we should generate the transmission of the other channels. Although Eq. (6) provides the relation of the three color channels, the reliability of the attenuation ratios relies on the accurate estimating of B .

Thus, we cannot get the accurate relationships only from Eq. (6). For instance, the smaller λ_g makes the range of t_g smaller, which reduces the contrast of the green channel of the image. Conversely, the larger λ_g makes the range of t_g close to t_r (with the large range), which can produce dark or saturated recovered pixels. So, we redefine the ratios λ'_c , $c \in \{r, g, b\}$ (λ'_r represents the self-adjust ratio) to adjust the transmission. According to Eq. (1) and (3), there are saturation constraints for the restored image:

$$0 \leq \frac{I_c(x) - B_c}{K \cdot \hat{t}_r^n(x)^{\lambda'_c}} + B_c \leq 1, \quad c \in \{r, g, b\}. \quad (20)$$

Then, we get:

$$\begin{cases} \lambda'_c \geq \ln(\frac{I_c(x) - B_c}{K(1 - B_c)}) / \ln(\hat{t}_r^n(x)) + \varepsilon_c & \text{if } I_c(x) > B_c \\ \lambda'_c \leq \ln(\frac{B_c - I_c(x)}{K \cdot B_c}) / \ln(\hat{t}_r^n(x)) + \varepsilon_c & \text{if } I_c(x) < B_c, \end{cases} \quad (21)$$

where we limit λ'_c in the range $[\lambda_c, 1]$, and set $\lambda_r = \max(\lambda_g, \lambda_b)$. Since these are strict constraints for the restored image, we use a tolerance of ε_c to ensure high contrast. In this paper, we choose ε_c which empirically makes 8% of recovered pixels exceed the limitations for each color channel. Hence, we use the new rates to adjust the transmission of each channel.

C. Scene Radiance Restoration

Once the waterlight and the final transmission are estimated, the scene radiance J can be restored by:

$$J_c(x) = \frac{I_c(x) - B_c}{\max(K \cdot \hat{t}_r^n(x)^{\lambda'_c}, t_0)} + B_c, \quad c \in \{r, g, b\}. \quad (22)$$

where $t_0 = 0.1$ [3]. Because some recovered images look dim, we use a global linear contrast stretch (clipping 0.5% the darker and brighter pixels) for display only in qualitative comparison, following the procedure explained in [17].

V. EXPERIMENT RESULTS

In this section, to assess the performance of the proposed method, we compared our underwater image restoration method against state-of-the-art IFM based methods: MIP-based [4], DCP-based (UDCP [8]), blurriness and light absorption based [9], and fixed attenuation-curve based (our previous work) [5] methods. For a fair assessment, all of the compared methods use codes provided by their authors and set default parameters. We evaluate our proposed method in three ways:

- 1) Qualitative comparison,
- 2) Quantitative no-reference comparison, and
- 3) Complexity analysis.

For the underwater testing images, we use 20 images with different light conditions and water tones from [4], [7], [11], [20]–[22] for evaluation as shown in Fig. 6.¹ We use the same parameters in our method for all of the testing images.

¹The experiment for all 37 testing images (including 17 images that are not shown in the paper from [4], [7], [11], [20], and [21]) has been described in detail in Part A of the supplemental material. See the link: <http://www.ntu.edu.sg/home/elpchau/underwater.zip>



Fig. 6. Sample testing images. Left to right, then top to bottom corresponds to “Image-1” to “Image-20”, respectively.

For waterlight estimation, we use 6-by-6 patches and set TV threshold as 0.9. N is a parameter that makes the intersection’s elements larger than 1. In order to find the curves, we set the number of clusters equal to 900 for the underwater image, and 3600 for the synthetic image. In Eq. (15), we set $\lambda = 0.05$ and scale $1/\sigma_r^2(x)$ to be in the range $[0, 1]$ as [17].

A. Qualitative Assessment

In the subjective visual comparison, we choose four representative underwater images (Image-1, 5, 10, 12) from Fig. 6, and use jet colormap to display the estimated transmission of the image. (For those methods producing three transmission maps, we show the green channel’s transmission.) In addition, we also show results of the estimated waterlight by each method. The method in [4] estimates the transmission firstly and finds a pixel with the minimum transmission as the waterlight. UDCP estimates the waterlight via finding the brightest pixel in the underwater dark channel. The method in [9] proposed a more reliable waterlight estimation method based on image blurriness and variance. Unlike other methods, we find it based on the observation of light attenuation in the water and low variance of the background. The results are shown in Fig. 7, where, for the four testing images, the estimated waterlights are presented in the first row, and the corresponding restored images and the estimated transmission are illustrated in the second and third rows.

In the turbid greenish underwater image with the bright background as shown in Image-1 of Fig. 7, all methods have similar results of the waterlight, which means MIP-based, DCP-based, blurriness-based and our methods are valid in the image with the bright background. However, MIP [4] has high values of the transmission and erroneously ignores the attenuation of the distance from the camera to the closest scene point, which leads to the remained green veil. Slightly better than that, UDCP [8] and [9] remove the veil marginally due to an underestimation of distance. Fixed-attenuation-curve based [5] and the proposed method can generate more satisfactory restoration results. Furthermore, our proposed method can recover more red color than [5] because of the effect of attenuation factor estimation in our method.

Image-5 of Fig. 7 illustrates a relative clear image with the bright foreground and dark background, which makes UDCP [8] invalid and has a brighter waterlight located in foreground area. The other three methods have more accurate results of the waterlight. The waterlight of our method is close to that of [9] with the darker color. Darker values of waterlight can increase the intensity in restored image. On the contrary, bright waterlight of [8] make the image dark, especially in the background area. So, our method and [5] can increase the intensity of the background and improve the contrast of the image by a better transmission estimation.

Similarly, our method can enhance more red color than [5]. Although [9] has a good transmission of the red channel, but it relied too heavily on the attenuation rates (Eq. (6)) to calculate the transmission of blue and green channels, which turn out to reduce the contrast.

For the shallow sea image (Image-10 of Fig. 7) with some reflection of light on the surface of water and sands in the seabed, UDCP [8] selects the bright pixels color as its waterlight that is located on the surface of the water. With the same result, the restored image of UDCP looks so dark both in the foreground and background. The blurriness-based method [9] can achieve satisfactory performance in this scenario. MIP [4] and Fixed-attenuation-curve based [5] methods fail in the background and bring many noises because the overestimated transmission of background enlarges the fluctuation of color in the restored image. In the proposed method, we add saturation constraints to adjust the transmission, which can reduce the noise when increasing the contrast (the distant coral reefs).

Image-12 of Fig. 7 shows the close shot without the background of infinity that gives a challenge to the waterlight estimation. UDCP [8] finds the brightest pixels as the waterlight among all methods, followed by [4], the proposed method and [9]. The result of UDCP has a good contrast but looks bluish. The result of our proposed method outperforms others in respect of the contrast and color correction. The comparisons of visual results by different methods are shown in Fig. 8. As can be seen in Fig. 7 and Fig. 8, compared with other methods, our proposed method can obtain better results and reduce the noises.

Although our approach is built on IFM and we compare it with the IFM-based methods, we still intend to compare it with the ACE method in the reference [10] which is a non-IFM image enhancement technique as shown in Fig. 9. The experimental results show that ACE cannot get a consistent color correction for Image-5 and Image-10, especially for distant coral reefs, and the contrast of the proposed outperforms the ACE method.

B. Quantitative Assessment

In addition to the above subjective visual comparison, the underwater image quality metrics (UIQM) [9], [23] measurement is utilized to evaluate the performance of the above mentioned methods. The UIQM measurement is composed of underwater image colorfulness measure (UICM), underwater image sharpness measure (UISM), underwater image contrast measure (UIConM). UIQM is the linear combination of the color, sharpness and contrast measures. UIQM is calculated as follows:

$$\text{UIQM} = c_1 \cdot \text{UICM} + c_3 \cdot \text{UISM} + c_1 \cdot \text{UIConM}, \quad (23)$$

where the default coefficients $c_1 = 0.0282$, $c_2 = 0.2953$ and $c_3 = 3.5753$.

The higher value of the UIQM stands for the better performance. In our experiments, we set the parameters $\alpha_L = \alpha_R = 0.1$ when calculating UICM. The patch size is set to 8×8 and the coefficients $\delta_1 = 0.299$, $\delta_2 = 0.587$ and $\delta_3 = 0.114$ in UISM. For the sample testing images,

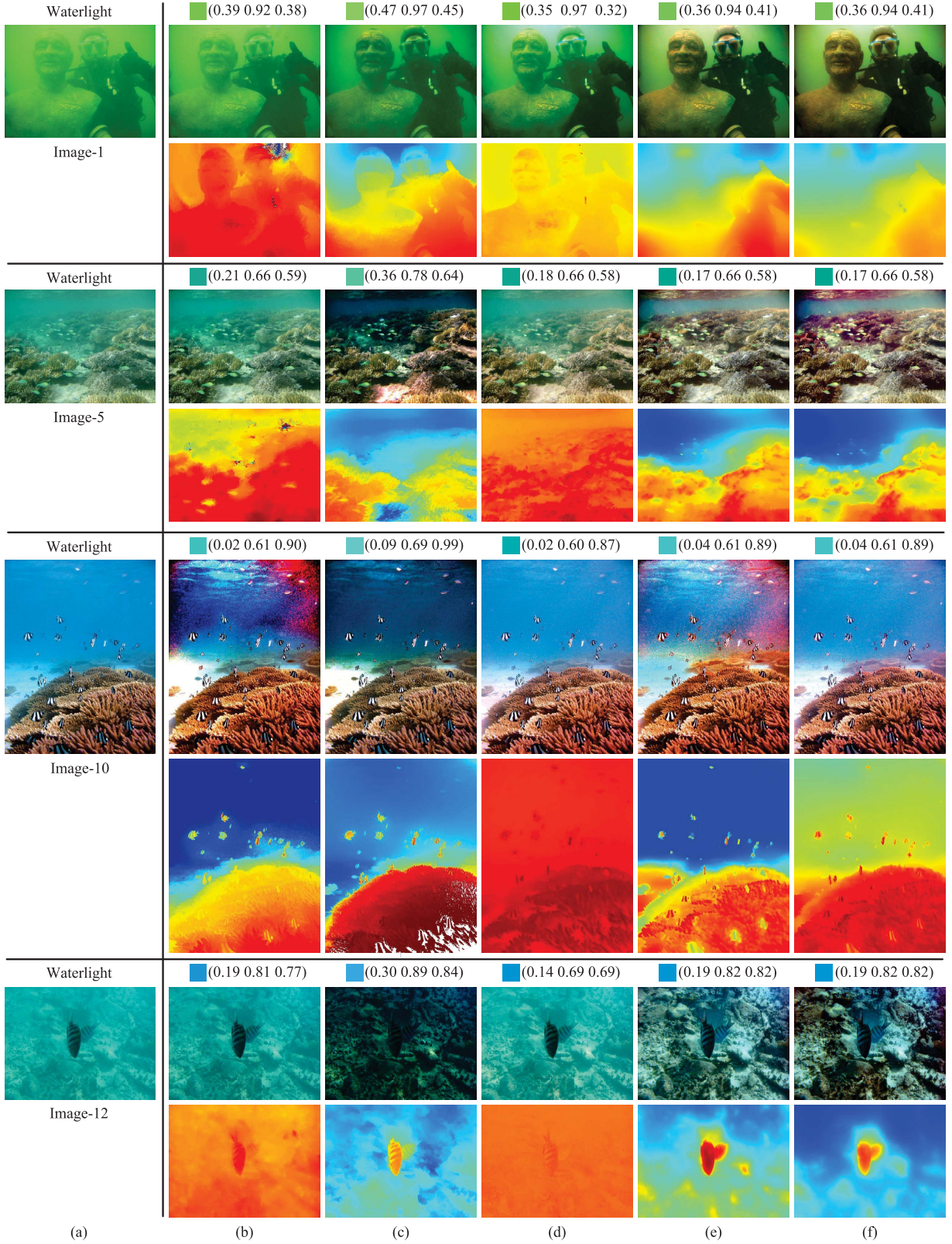


Fig. 7. The visual comparison of four underwater images with different scenes. (a) The original image. The restored results, and the corresponding waterlight and transmission yielded by: (b) MIP [4], (c) UDCP [8], (d) blurriness-based method [9], (e) fixed-attenuation-curve method [5], (f) the proposed method (adaptive attenuation-curve).

Table I shows the UIQM values of the restored images by different methods. It demonstrates our method performs better in most cases.

C. Complexity Analysis

Our proposed underwater restoration approach is non-local pixel based, which is more efficient than those

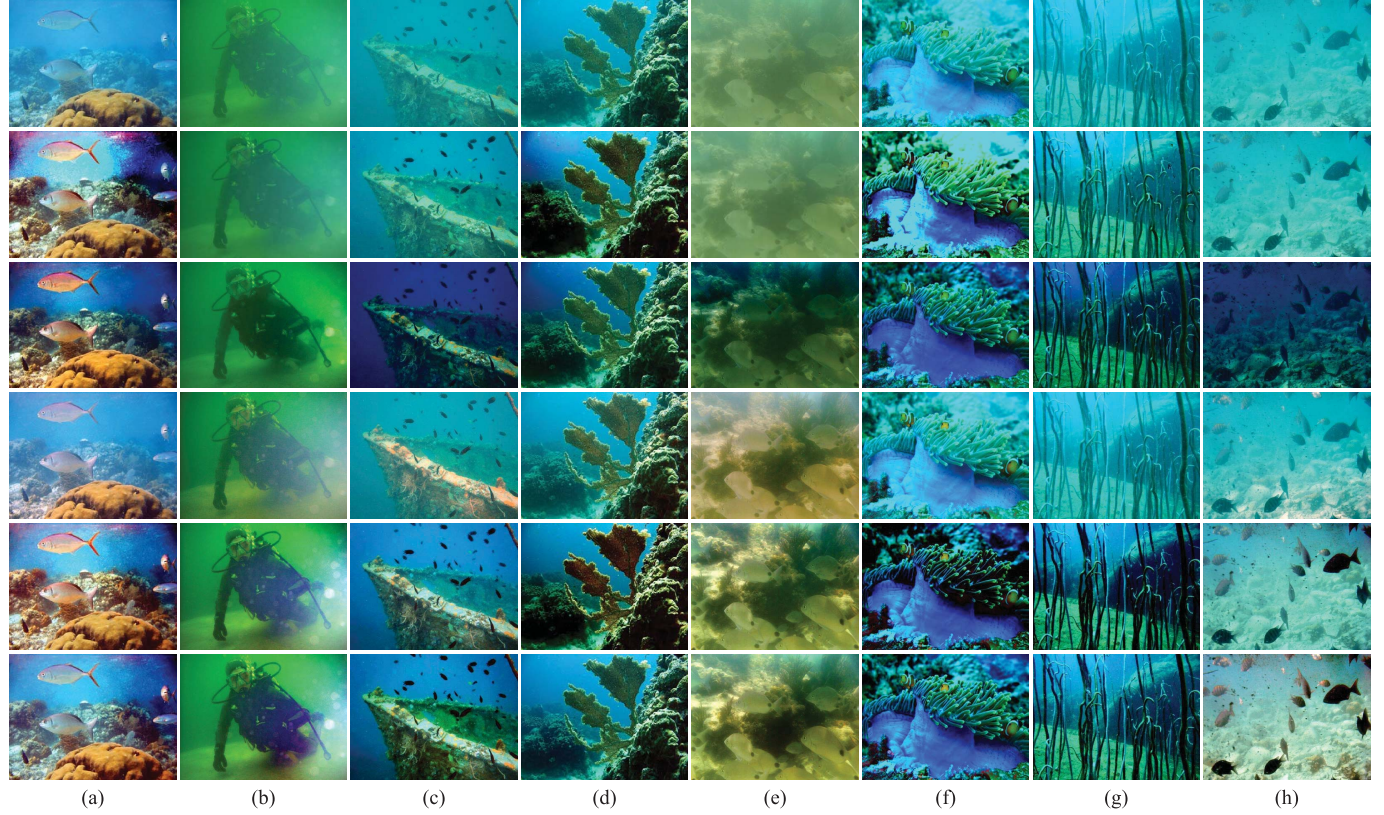


Fig. 8. Comparisons of visual results by different methods. Row 1 is the input images; row 2 is the results of MIP [4]; row 3 is the results of UDCP [8]; row 4 is the results of the blurriness-based method [9]; row 5 is the results of the fixed-attenuation-curve based method [5]; row 6 is the results of our proposed method.

TABLE I
UIQM VALUES AMONG DIFFERENT METHODS

# Image	UIQM				
	[4]	[8]	[9]	[5]	Ours
1	1.1112	2.5157	2.3295	3.175	3.5887
2	4.5072	3.9947	4.7803	4.2967	4.5907
3	5.033	5.0559	4.4216	5.3502	5.2595
4	2.5981	4.2301	3.7809	4.1648	4.3133
5	4.0478	4.3145	4.2518	4.785	4.7567
6	0.6235	3.4309	2.7203	3.6758	3.9611
7	2.3868	2.1942	2.6519	2.698	2.9193
8	4.0743	4.2122	4.3741	3.8583	3.9894
9	3.2611	2.2732	3.6926	3.718	3.6461
10	4.7316	4.5172	4.5156	5.0294	5.0132
11	0.6973	3.3234	3.3979	2.5245	3.8666
12	2.4927	3.0643	2.7725	4.1311	4.0734
13	4.0572	4.4427	4.9488	4.8074	4.8536
14	3.2528	3.0608	2.5855	3.0244	3.3188
15	2.8381	3.1636	2.8087	3.096	3.4492
16	4.2071	4.1544	4.5712	4.5607	4.5946
17	1.8945	2.8919	2.2753	4.2789	4.4814
18	4.5493	3.7596	4.5628	4.9285	4.8462
19	2.5251	2.7899	3.0232	3.3851	3.4149
20	4.8277	3.7059	5.0385	4.3988	4.779
Average	3.1858	3.5548	3.6752	3.9943	4.1858

patch-based methods. Because we estimate per-pixel transmission for each curve, given an image with the size of $m \times n$, the computational complexity of initial transmission estimation is $O(m \times n)$. According to the analysis of [17], the computational complexity of refining transmission is

TABLE II
COMPUTATION TIME COMPARISON

Image Resolution	[4]	[8]	[9]	Ours
512 × 384	431.19 s	3.08 s	22.38 s	1.78 s
640 × 480	881.83 s	4.80 s	34.98 s	2.18 s
960 × 720	3714.58 s	10.50 s	81.72 s	5.07 s
1024 × 768	4605.45 s	12.65 s	90.69 s	5.52 s

also $O(m \times n)$. Besides, KD-Tree is fast when we use predefined tessellation to cluster pixels. As shown in Table II, we present the computation time comparison with MIP-based method [4], UDCP [8] and blurriness and light absorption based method [9] in MATLAB R2015b with a CPU (Intel Xeon E5-1630 v3, 3.7 GHz). The experimental results show our method is much faster than the others on different image resolutions.

D. Other Applications in the Atmosphere

The proposed methods can also be extended to the degraded images captured in the atmosphere, such as hazy images. Our proposed prior is for underwater images which would not imply the optimized performance in the atmosphere model. However, we would still like to compare our approach with some state-of-the-art dehazing methods [3], [17] using a synthetic dataset [18]. For hazy images, there is an assumption that the attenuation coefficients of color channels are equal

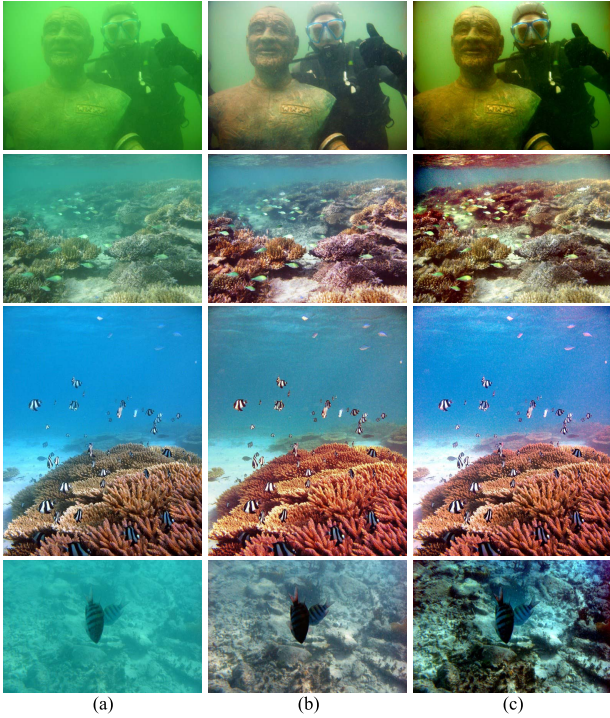


Fig. 9. Comparison with the non-IFM image enhancement method. (a) The input images; (b) the results of ACE [10]; (c) the results of the proposed method. Row 1 is for Image-1 numbered in Fig. 6; row 2 is for Image-5; row 3 is for Image-10; row 4 is for Image-12.

TABLE III

COMPARISON OF L1 ERRORS OVER SYNTHETIC HAZY IMAGES. THE TABLE PRESENTS THE L1 ERRORS OF THE ESTIMATED TRANSMISSION (LEFT VALUE) AND THE DEHAZED IMAGES (RIGHT VALUE)

	He's [3] Dark Channel	Berman's [17] Haze-Line	Our proposed Attenuation-Curve
Church	0.070 / 0.048	0.047 / 0.032	0.066 / 0.047
Couch	0.069 / 0.041	0.051 / 0.031	0.037 / 0.022
Flower1	0.190 / 0.098	0.061 / 0.022	0.040 / 0.015
Flower2	0.203 / 0.094	0.115 / 0.045	0.079 / 0.032
Lawn1	0.118 / 0.063	0.032 / 0.026	0.042 / 0.031
Lawn2	0.115 / 0.066	0.041 / 0.031	0.059 / 0.042
Mansion	0.074 / 0.043	0.080 / 0.049	0.074 / 0.046
Moebius	0.235 / 0.146	0.153 / 0.081	0.088 / 0.042
Raindeer	0.127 / 0.068	0.089 / 0.045	0.088 / 0.042
Road1	0.097 / 0.051	0.058 / 0.040	0.064 / 0.045
Road2	0.087 / 0.056	0.062 / 0.042	0.062 / 0.041
Average	0.126 / 0.070	0.072 / 0.040	0.066 / 0.037



Fig. 10. Results of three images taken in the atmospheric environment. Row 1 is the hazy images and row 2 is the restored images by the proposed method.

to each other. So, we set $t_r = t_g = t_b$ in the model (Eq. (1)). Table III presents the L1 errors on non-sky pixels of the transmission maps and the dehazed images. Our method

outperforms other methods in both the estimated transmission maps and the restored images in most cases.² Figure 10 presents the experimental results of three images taken in the atmospheric environment. It shows that our method can not only improve the contrast and visibility in the distant area but also achieve good color saturation.

VI. CONCLUSION

In this paper, we introduced a novel adaptive attenuation-curve prior. For underwater images, the pixels from the same cluster can form a power function curve in RGB space. Compared with the fixed curve, the adaptive curve can model the attenuation process of light for different underwater environments. We proposed an effective method to estimate the waterlight by the smoothness property and the attenuation of light. Through the prior, we clustered the pixel values of the image into the curves and estimated the transmission for each curve. To reduce the over saturation and noise in the restored images, we exploited the saturation constraints to adjust the transmission of the three color channels. The qualitative results demonstrated our proposed method improves the contrast and removes the color cast, and suppresses the noises. Besides, the quantitative results showed our method outperforms state-of-the-art approaches.

The theoretical ideas presented in this manuscript have been applied to real-world underwater images. Moreover, we will give some prospect for theoretical and practical issues, which are worth investigating further. On the theoretical side, we can more accurately estimate the attenuation ratios between color channels, since these ratios can greatly affect the accuracy of the transmission estimation. On the practical side, a parallel acceleration for system realization can be designed. Because our approach is pixel based and the transmission estimation for pixels for one curve is independent to another curve, it is suitable for parallel processing.

ACKNOWLEDGMENT

The authors would like to thank the Singapore Maritime Institute (SMI) for kindly funding this research project and Fugro Subsea Technologies Pte Ltd. providing technical platform for testing and evaluation under the SMI Deepwater Technology R&D Programme.

REFERENCES

- [1] Y. Y. Schechner and N. Karpel, "Clear underwater vision," in *Proc. IEEE Conf. Comput. Vis. Pattern Recognit.*, vol. 1, Jun. 2004, pp. 536–543.
- [2] J. Y. Chiang and Y.-C. Chen, "Underwater image enhancement by wavelength compensation and dehazing," *IEEE Trans. Image Process.*, vol. 21, no. 4, pp. 1756–1769, Apr. 2012.
- [3] K. He, J. Sun, and X. Tang, "Single image haze removal using dark channel prior," *IEEE Trans. Pattern Anal. Mach. Intell.*, vol. 33, no. 12, pp. 2341–2353, Dec. 2011.
- [4] N. Carlevaris-Bianco, A. Mohan, and R. M. Eustice, "Initial results in underwater single image dehazing," in *Proc. IEEE OCEANS*, Sep. 2010, pp. 1–8.
- [5] Y. Wang, H. Liu, and L.-P. Chau, "Single underwater image restoration using attenuation-curve prior," in *Proc. IEEE Int. Symp. Circuits Syst.*, May 2017.

²The corresponding estimated transmission maps and recovered images for Table III can be found in Part B of the supplemental material. See the link: <http://www.ntu.edu.sg/home/elpchau/underwater.zip>

- [6] H. Wen, Y. Tian, T. Huang, and W. Gao, "Single underwater image enhancement with a new optical model," in *Proc. IEEE Int. Symp. Circuits Syst.*, May 2013, pp. 753–756.
- [7] A. Galdran, D. Pardo, A. Picón, and A. Alvarez-Gila, "Automatic red-channel underwater image restoration," *J. Vis. Commun. Image Represent.*, vol. 26, pp. 132–145, Jan. 2015.
- [8] P. Drews, E. do Nascimento, F. Moraes, S. Botelho, and M. Campos, "Transmission estimation in underwater single images," in *Proc. IEEE Int. Conf. Comput. Vis. Workshops*, Dec. 2013, pp. 825–830.
- [9] Y.-T. Peng and P. C. Cosman, "Underwater image restoration based on image blurriness and light absorption," *IEEE Trans. Image Process.*, vol. 26, no. 4, pp. 1579–1594, Apr. 2017.
- [10] P. Getreuer, "Automatic color enhancement (ACE) and its fast implementation," *Imag. Process. Line*, vol. 2, pp. 266–277, Nov. 2012.
- [11] C. Ancuti, C. O. Ancuti, T. Haber, and P. Bekaert, "Enhancing underwater images and videos by fusion," in *Proc. IEEE Conf. Comput. Vis. Pattern Recognit.*, Jun. 2012, pp. 81–88.
- [12] X. Fu, P. Zhuang, Y. Huang, Y. Liao, X.-P. Zhang, and X. Ding, "A retinex-based enhancing approach for single underwater image," in *Proc. IEEE Int. Conf. Image Process.*, Oct. 2014, pp. 4572–4576.
- [13] E. H. Land and J. J. McCann, "Lightness and Retinex theory," *J. Opt. Soc. Amer.*, vol. 61, no. 1, pp. 1–11, 1971.
- [14] W. E. K. Middleton, *Vision Through the Atmosphere*. Toronto, ON, Canada: Univ. Toronto Press, 1952.
- [15] R. W. Gould, R. A. Arnone, and P. M. Martinolich, "Spectral dependence of the scattering coefficient in case 1 and case 2 waters," *Appl. Opt.*, vol. 38, no. 12, pp. 2377–2383, 1999.
- [16] X. Zhao, T. Jin, and S. Qu, "Deriving inherent optical properties from background color and underwater image enhancement," *Ocean Eng.*, vol. 94, pp. 163–172, Jan. 2015.
- [17] D. Berman, T. Treibitz, and S. Avidan, "Non-local image dehazing," in *Proc. IEEE Conf. Comput. Vis. Pattern Recognit.*, Jun. 2016, pp. 1674–1682.
- [18] R. Fattal, "Dehazing using color-lines," *ACM Trans. Graph.*, vol. 34, no. 13, 2014, Art. no. 13.
- [19] Z. Farbman, R. Fattal, D. Lischinski, and R. Szeliski, "Edge-preserving decompositions for multi-scale tone and detail manipulation," *ACM Trans. Graph.*, vol. 27, no. 3, 2008, Art. no. 67.
- [20] R. Fattal, "Single image dehazing," *ACM Trans. Graph.*, vol. 27, no. 3, 2008, Art. no. 72.
- [21] S. Emberton, L. Chittka, and A. Cavallaro, "Hierarchical rank-based veiling light estimation for underwater dehazing," in *Proc. Brit. Mach. Vis. Conf.*, 2015, p. 125.1–125.12.
- [22] J. Xiao, J. Hays, K. A. Ehinger, A. Oliva, and A. Torralba, "Sun database: Large-scale scene recognition from abbey to zoo," in *Proc. IEEE Conf. Comput. Vis. Pattern Recognit.*, Jun. 2010, pp. 3485–3492.
- [23] K. Panetta, C. Gao, and S. Agaian, "Human-visual-system-inspired underwater image quality measures," *IEEE J. Ocean. Eng.*, vol. 41, no. 3, pp. 541–551, Jul. 2016.



Yi Wang received the B.Eng. and M.Eng. degrees from the School of Electronics and Information, Northwestern Polytechnical University, Xi'an, China, in 2013 and 2016, respectively. He is currently pursuing the Ph.D. degree with Nanyang Technological University, Singapore. He is currently a Research Associate with the School of Electrical and Electronic Engineering, Nanyang Technological University. His research interests include image processing and computer vision.



Hui Liu received the B.Eng. degree (Advanced Class) and the M.Eng. degree in communication engineering from Central South University in 2009 and 2012, respectively, and the M.Eng. degree from the School of Computer Engineering, Nanyang Technological University, in 2014. She was a Research Associate with the Maritime Institute, Nanyang Technological University, from 2014 to 2017. Her research interests include image and video processing.



Lap-Pui Chau (F'17) received the bachelor's degree from Oxford Brookes University in 1992, and the Ph.D. degree from The Hong Kong Polytechnic University in 1997. His research interests include fast visual signal processing algorithms, light-field imaging, video analytics for intelligent transportation system, and human motion analysis. Dr. Chau was a Steering Committee Member of the IEEE TRANSACTIONS FOR MOBILE COMPUTING from 2011 to 2013. He was an IEEE Distinguished Lecturer from 2009 to 2016. He served as an Associate Editor of the IEEE TRANSACTIONS ON MULTIMEDIA, the IEEE SIGNAL PROCESSING LETTERS, and the IEEE TRANSACTIONS ON CIRCUITS AND SYSTEMS FOR VIDEO TECHNOLOGY. He is currently serving as an Associate Editor of the IEEE TRANSACTIONS ON CIRCUITS AND SYSTEMS-II, the IEEE TRANSACTIONS ON BROADCASTING, and *The Visual Computer* (Springer Journal).

Dr. Chau was the Chair of the Technical Committee on Circuits and Systems for Communications of the IEEE Circuits and Systems Society from 2010 to 2012. He was a General Chair of the IEEE International Conference on Digital Signal Processing in 2015 and the International Conference on Information, Communications and Signal Processing in 2015. He was a Program Chair at the International Conference on Multimedia and Expo in 2016, the Visual Communications and Image Processing in 2013, and the International Symposium on Intelligent Signal Processing and Communications Systems in 2010.